Walter, Phelan. Published in Continental Shelf Research 116. March, 2016. 42-53.

Internal bore seasonality and tidal pumping of subthermocline waters at the head of the Monterey submarine canyon

Ryan K. Walter [a,*], P. Joe Phelan [b]

[a] Physics Department, California Polytechnic State University, San Luis Obispo, CA, USA
[b] Tenera Environmental, San Luis Obispo, CA, USA

A B S T R A C T

This study utilizes more than a year of observations made in shallow waters (~30 m) at the head of the Monterey Submarine Canyon to assess variability in the physical environment and internal bore field. The interaction of the internal tide with the canyon rim results in a semidiurnal tidal period pumping of cold–water masses (subthermocline waters) onto the adjacent shelf (i.e., internal bores). These internal bores are shown to be significantly coherent with the local sea surface height with minimal spatial variability when comparing two sites near the canyon head region. During the summer months, and periods of strong regional wind-driven upwelling and shoaling of the offshore thermocline, the canyon rim sites display elevated semidiurnal temperature variance. This semidiurnal variability reaches its annual minimum during the winter months when the regional upwelling favorable winds subside and the offshore thermocline deepens. Additionally, the observed internal bores show a distinct asymmetry between the leading (gradual cooling with velocities directed onto the shelf) and trailing edges (sharp warming with velocities directed into the canyon). It appears that the semidiurnal internal tide at the canyon head is a first-order control on the delivery of subthermocline waters to the nearshore coastal environment at this location.

1. Introduction

Internal gravity waves are a widespread feature of the coastal ocean and are generated in stably stratified waters when surface (barotropic) tides flow over sloping bottom topography (Garrett and Kunze, 2007). This process displaces density surfaces (isopycnals) vertically at tidal frequencies, and thus these features have been termed internal tides (i.e., internal gravity waves at a tidal frequency). Large amplitude internal waves and tides are a ubiquitous phenomenon along the continental margins of Monterey Bay, CA and are dominated by the semidiurnal (M_2 tidal constituent) frequency component (Shea and Broenkow, 1982; Petruncio et al., 1998; Kunze et al., 2002; Zhao et al., 2012; Hall et al., 2014; etc.). Semidiurnal internal tides in this region are also enhanced by the presence of the Monterey Submarine Canyon (MSC), one of the largest submarine canyons on the west coast of the United States. The MSC acts to trap and focus surface and internal tide energy in the canyon interior, resulting in internal tides that are an order of magnitude more energetic than the open ocean internal wave field (Kunze et al., 2002). Numerical modeling efforts and field observations have documented a substantial incident semidiurnal baroclinic energy flux at the canyon mouth and have concluded that the main offshore generation site is likely near the Sur Slope/Ridge; however, additional generation and interaction between the remotely and locally generated fields likely occurs in the canyon interior and shelf break region (Jachec et al., 2006; Petruncio et al., 1998, 2002; Kunze et al., 2002; Carter, 2010; Kelly and Nash, 2010; Kang and Fringer, 2012; etc.).

The internal tide also manifests itself shoreward of the canyon interior through a process known as tidal pumping (Shea and Broenkow, 1982; Petruncio et al., 1998, 2002). Tidal pumping refers to a process whereby the thermocline crests the shelf/canyon edge due to water displacement associated with the internal tide [see Shea and Broenkow (1982) for a description of this process in terms of volume convergence/divergence and continuity and their Fig. 7 for a schematic]. The resulting uplifted cold–water masses are transported onto the adjacent shelf along the canyon rim and lead to the formation of higher frequency nonlinear internal waves (NLIWs), solitons, and boluses (bores) (Venayagamoorthy and Fringer, 2007). In this contribution, we will refer to the cold–water surges/boluses as bores following the non-canonical description in Walter et al. (2012) (see Section 3.2), even though the typical (canonical) bore has an initial shock-like front that is not seen in the features described here (see Venayagamoorthy and Fringer,

* Corresponding author.
E-mail address: rkwalter@calpoly.edu (R.K. Walter).

2007; Walter et al., 2012; Martini et al., 2013; and the references therein). The presence of NLIWs and bores in the Monterey Bay region has been documented in field observations near the canyon edge (Shea and Broenkow, 1982; Carter and Gregg, 2002; Carter et al., 2005), as well as on the adjacent shelf (Storlazzi et al., 2003; Woodson et al., 2011; Walter et al., 2012, 2014a, 2014b; Cheriton et al., 2014a, 2014b). The documented cold–water features near the canyon edge appear to be correlated to the surface tide (e.g., 1 week observations of Shea and Broenkow (1982)), while the features on the shelf occur intermittently and are not well correlated with surface tides (Booth et al., 2012; Walter et al., 2012). The latter is consistent with observations from other continental margin locations (Kelly and Nash, 2010; Nam and Send, 2011; see also Nash et al. (2012)).

NLIWs and bores are ubiquitous phenomena along continental margins and are known to have a significant effect on shelf circulation and exchange processes, turbulent dissipation and mixing dynamics, nutrient cycling, larval transport, sediment transport, and intermediate nepheloid layers (Shea and Broenkow, 1982; Pineda, 1994; Boehm et al., 2002; Carter and Gregg, 2002; Carter et al., 2005; Woodson et al., 2011; Walter et al., 2012, 2014a, 2014b; Cheriton et al., 2014a; Suanda et al., 2014; etc.). Furthermore, tidal pumping and the NLIW/bore field can significantly enhance the delivery of subthermocline waters to the nearshore, a process that is critical for understanding dissolved oxygen (DO) variability and coastal hypoxia, the transport of low pH waters to the nearshore and ocean acidification, and the design of future desalination plants that seek to access deep subthermocline waters (Booth et al., 2012; Walter et al., 2014b). NLIWs and bores in the stratified coastal ocean thus represent an important scientific and practical problem, with considerable implications for many biological and physical processes along coastal boundaries.

There is a growing number of field observations and numerical modeling efforts aimed at understanding the internal tide field and NLIWs/bores in the Monterey Bay region (Shea and Broenkow, 1982; Petruncio et al., 1998, 2002; Carter and Gregg, 2002; Kunze et al., 2002; Storlazzi et al., 2003; Carter et al., 2005; Jachec et al., 2006; Carter, 2010; Hall and Carter, 2011; Kang and Fringer, 2012; Zhao et al., 2012; Walter et al., 2012, 2014a, 2014b; Hall et al., 2014; Cheriton et al., 2014a, 2014b; etc.). Yet, previous computational studies necessarily concentrated on simplified and idealized setups. Likewise, the majority of observational studies concentrated on deeper canyon waters (100–1000+ m depths) over shorter time periods (days to weeks), or focused their efforts away from the canyon edge. Field observations near the canyon head, or along the canyon rim, were restricted to 1–2 week study periods using shipboard surveys and moored instruments (Shea and Broenkow, 1982; Carter and Gregg, 2002; Carter et al., 2005). Indeed, there is a paucity of long-term observations of NLIWs and bores near the MSC head in shallower waters, even though elevated semidiurnal internal wave energy has been observed near the head of several other canyon locations worldwide (cf. Petruncio et al. (1998) and the references therein; Hall et al. (2014) and the references therein). We also surmise that the canyon head could potentially be the site of enhanced delivery of subthermocline waters to nearshore shelf regions with important ecological habitats such as kelp forests (*Macrocystis pyrifera*) (e.g., see bore directionality in Walter et al. (2012)).

Long-term observations are critical to understanding the physical environment and internal tide field at the head of the canyon. For example, recent longer-term observations in the canyon and on the shelf have demonstrated the importance of wind-driven upwelling cycles and seasonality on the propagation and character of internal waves. Observations made over a two month period (mid-February to mid-April) by Zhao et al. (2012) and Hall et al. (2014) in deeper canyon waters (e.g., 150–600 m depths) revealed that changes in stratification driven by a seasonal shift in wind-driven upwelling resulted in changes to the behavior of the internal tide (i.e., progressive versus standing wave) and patterns of velocity, displacement, and energy flux in the upper reaches of the MSC. Walter et al. (2014b) showed that the strength and structure of nearshore internal bores in southern Monterey Bay was modulated by mid-shelf stratification and wind-driven upwelling/relaxation cycles. Cheriton et al. (2014b) illustrated that upwelling events led to the infiltration of dense water onto the shelf, which created a near-bottom pycnocline and enabled the propagation of NLIWs onto the southern shelf. The authors concluded that regional upwelling dynamics partially control the ability of internal waves to propagate through continental shelf waters. The recent review by Washburn and McPhee-Shaw (2013) discusses how seasonal upwelling, and transitions between upwelling/downwelling events and changes in stratification, may lead to the modulation of internal wave transport and the delivery of subthermocline waters to shallow coastal regions. While the above-mentioned studies have revealed significant insight into the influence of regional upwelling cycles on internal wave structure and transport, the studies were limited to observations over (up to) several months during a specific upwelling seasonality regime (García-Reyes and Largier, 2012). Observations encompassing a complete annual record documenting the seasonal variability in upwelling winds and the subsequent response of shallow water NLIWs and bores are needed as they would provide a seasonal context for this phenomenon. This will provide a basis for insight into a host of physical processes (see above) that underpin and interact with the coastal ecosystem, for example through the seasonal modulation of the flux of subthermocline waters (high nutrients, low DO/pH) to the nearshore.

In this study, we take advantage of long-term moored measurements made in relatively shallow waters (~30 m depth) at the head of the MSC in order to characterize the physical environment and the seasonality of NLIWs/bores. We expand on the observations of Shea and Broenkow (1982) with a more spatiotemporally resolved data set and a more detailed look into the dynamics at the head of the MSC. The spatial and temporal variability of the NLIW/bore field and the subsequent impact on the transport of subthermocline waters is also examined. Extension of the results to other locations, recommendations for future work, and ecological implications are briefly discussed.

2. Experimental setup and methods

2.1. Study site

Monterey Bay is a semi-enclosed embayment located along the central coast of California and within the highly productive CCLME (Fig. 1). It is also a biologically diverse marine system located within the Monterey Bay National Marine Sanctuary, and it is home to some of the world's largest kelp forests (*Macrocystis pyrifera*) and large commercial fisheries. The bay features a narrow shelf near the canyon head region where the canyon rim is closest to the shoreline and a relatively broad shelf elsewhere with roughly 80% of the bay shallower than 100 m (Breaker and Broenkow, 1994). The narrow shelf is cut by a system of submarine canyons, the largest of which is the MSC. The MSC is one of the largest submarine canyons on the west coast of the United States. The main axis of the MSC bisects through the approximate center of the bay and terminates at the canyon head, which is located within 100 m of the shore and entrance to the Moss Landing Harbor (Fig. 1).

General physical oceanographic conditions include a mixed semidiurnal tide with currents dominated by the M_2 (~12.42 h period) tidal constituent (Breaker and Broenkow, 1994). The intense

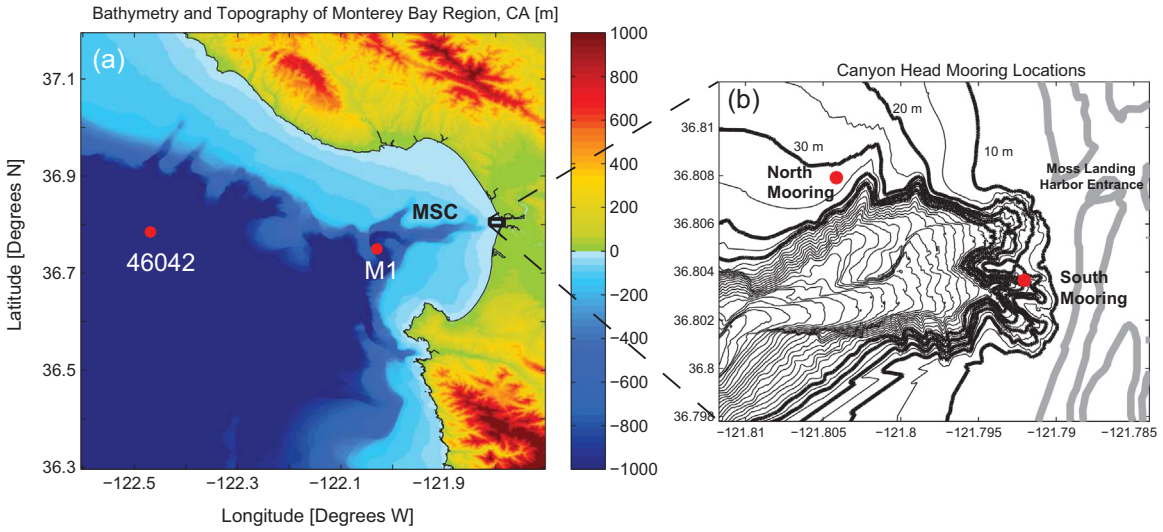

Fig. 1. (a) Bathymetry and topography of the Monterey Bay region highlighting the location of buoy-data used in the study (red circles), the Monterey Submarine Canyon (MSC), and the nearshore canyon head study site (black box). (b) Canyon head study site showing the nearshore mooring locations (red circles). Isobath contours are shown every 5 m from 10 m to 200 m, while the bold contour lines delineate the 10, 20, 30, 40, and 50 m isobaths. Thick gray lines in (b) denote the shoreline. (For interpretation of the references to color in this figure legend, the reader is referred to the web version of this article.)

productivity of the CCLME, including Monterey Bay, is driven by seasonal upwelling, where along-shelf equatorward winds drive a net offshore (Ekman) transport of surface waters. This process is driven by the Coriolis force, and acts to bring deep, cold waters (nutrient-rich, low in DO/pH) to the surface. During the upwelling season in Monterey Bay (~March to October), regional northwesterly winds create a strong upwelling jet at Point Año Nuevo that advects southward across the mouth of the bay at the surface (Rosenfeld et al., 1994). Recent studies (Walter et al., 2014b; Cheriton et al., 2014b), including this one, suggest that the upwelling response inside the bay and on the shelf is partially due to the cross-margin tilting of isotherms (possibly due to current-driven geostrophic adjustment), which doesn't routinely manifest itself at the surface and results in changes to the vertical structure of stratification and the internal wave guide.

2.2. Setup

A set of moored instrument arrays were deployed in ~30 m of water along the canyon rim and near the head of MSC (Fig. 1b) in order to characterize the physical environment and internal tide field over a broad range of time scales. Both the North and South mooring sites were equipped with a vertical array of thermistors sampling at 10 min intervals. The South mooring contained five Onset Corporation HOBO StowAway TidbiT temperature loggers (0.2 °C accuracy) spaced 3.05 m (10 ft) apart and located at 0.9, 4.0, 7.0, 10.1, 13.1 mab (meters above the bed). The instruments were deployed 9 March 2012 and sampled nearly continuously until 2 July 2013. The North mooring contained Onset Corporation HOBO U24-002-C loggers (0.1 °C accuracy) located at 1.5 and 13.7 mab. The temperature loggers at the North canyon rim site sampled nearly continuously from 30 May 2012 to 13 March 2013.

An upward looking 600 kHz Nortek Aquadopp acoustic Doppler profiler (ADP) was deployed at both the North and South mooring sites. The ADPs were raised 0.6 mab with the first bin located at 2.1 mab and the instrument collecting velocity measurements throughout the water column in 1 m vertical bins. Unfortunately, the South mooring ADP suffered from sediment movement and instability at the canyon rim and the measurements were deemed unsalvageable (cf. Smith et al. (2005)). The North mooring ADP, which was co-located next to the temperature loggers, sampled at 1 Hz in 5 min bursts every 30 min. The instrument collected data nearly continuously from 3 October 2012 to 13 June 2013. Surface layer effects were accounted for by removing at least the top 10% of the water column plus an additional 1 m. Velocity measurements were rotated from magnetic coordinates into true north, east, and vertical velocity components based on the local magnetic declination.

Offshore wind vectors were obtained from the National Data Buoy Center (NDBC) 46042 buoy (Fig. 1a), located west of the mouth of Monterey Bay. The offshore vertical temperature structure was characterized using data from the Monterey Bay Aquarium Research Institute (MBARI) M1 mooring located at the mouth of Monterey Bay and the MSC (Fig. 1a). Temperature measurements were obtained at 10 min sampling intervals at the following depths: 1, 10, 20, 40, 60, 80, 100, and 150 m. Tidal height data over the length of the experiment was obtained from the National Oceanic and Atmospheric Administration (NOAA) Tides and Current station 9413450 located in Monterey Bay. The tidal height data was corroborated against the time-mean removed sea surface height data derived from the ADP pressure sensor during the period of deployment. All times referenced here are in Pacific Standard Time (PST), unless otherwise noted.

2.3. Methods

To analyze the frequency content of various time series, spectral calculations were carried out following standard methods using the fast Fourier transform (FFT) (Walter et al., 2011). The choice of window length for spectral calculations was determined by taking into account the length of the record, frequency resolution, frequency scales of interest, and the resulting number of degrees of freedom (DOF) used for confidence intervals. Hamming windows with 50% overlap were applied to decrease spectral leakage. Confidence intervals for spectra were calculated using a chi-square variable analysis and the “equivalent” number of DOF (EDOF). Confidence limits were calculated using the EDOF for the coherence analysis (Emery and Thomson, 2001).

Continuous wavelet transforms were utilized in order to examine the time-varying frequency content (i.e., power) of the internal waves (Davis et al., 2008; Wong et al., 2012). The non-stationary signals were decomposed into frequency-time space following the methods outlined in Torrence and Compo (1998). The Morlet wavelet was chosen as the mother wavelet function with a nondimensional frequency parameter (ω_0 as in Torrence and

Compo, 1998) set to be equal to six (Farge, 1992). The wavelet power spectrum is expressed as the magnitude of the wavelet transform squared, $W = |W_n(s)|^2$, where n is a localized time index and the wavelet scale (s) is nearly identical to the Fourier period. Wavelet power as a function of time over a particular band of scales (periods) s_1 to s_2 is quantified using the scale-averaged wavelet power:

$$\langle W(t)\rangle = \frac{\delta j \delta t}{C_\delta} \sum_{j=j1}^{j2} \frac{|W_n(s_j)|^2}{s_j}, \quad (1)$$

where δj is the scale resolution, δt is the sampling time interval, and C_δ is a reconstruction constant. Wavelet power significance is calculated by comparing it to a background model spectrum of red-noise. Additional details can be found in Torrence and Compo (1998).

3. Results and discussion

3.1. General observations

The time series of regional upwelling favorable winds (i.e., along-shore equatorward) highlights a seasonal cycle whereby upwelling winds are strongest from approximately March to October and subside during the winter months (Fig. 2a; García-Reyes and Largier, 2012). During the spring transition to strong upwelling favorable winds (~February to April), the offshore isotherms begin to shoal towards the surface as the water column cools. Following this transition, surface water temperatures begin to warm and the water column is marked by strong thermal stratification, with a subsequent deepening of isotherms and isohalines (isohalines not shown). As the upwelling winds begin to weaken and consistently reverse (i.e., downwelling) in the winter months, the water column warms and the thermocline deepens. The response of the offshore temperature structure to the seasonal changes in wind forcing is consistent with the long-term observations of Pennington and Chavez (2000). The upwelling wind record is also characterized by higher-frequency upwelling/relaxation cycles with upwelling favorable winds persisting for 1–2 weeks, followed by relaxation events lasting several days. In the context of wind-driven upwelling, we refer to a wind relaxation event as the decay or reversal of upwelling favorable winds (Send et al., 1987). Also evident in the temperature structure are changes in the offshore stratification and thermocline depth in response to the 1–2 week period upwelling/relaxation cycles (Walter et al., 2014b).

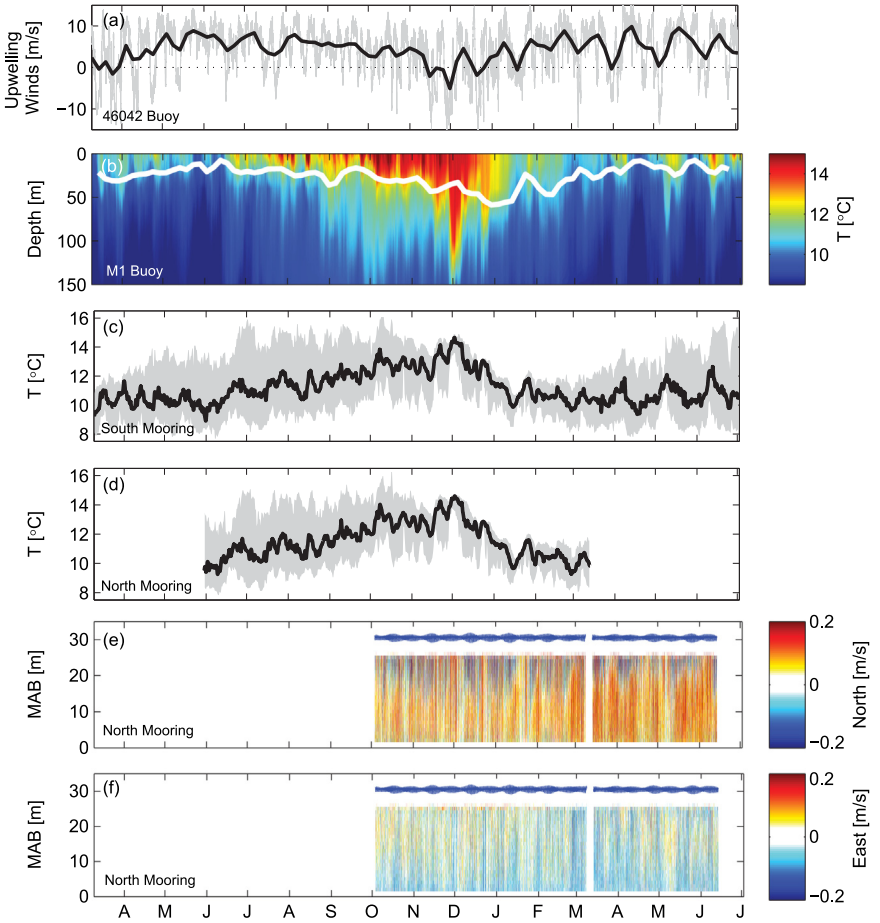

Fig. 2. Time series over the entire 2012–2013 study period. (a) Regional upwelling favorable winds (positive, gray line) from NDBC buoy 46042. The solid black line represents the 10 day windowed-mean (50% overlap between adjacent segments). (b) Offshore vertical temperature structure from MBARI M1 mooring (interpolated to 1 m and only the top 150 m of the water column shown). The solid white line represents the vertical location of the depth-averaged temperature from the South canyon head mooring. The line displayed is the 10 day windowed-mean (50% overlap between adjacent segments). (c) Daily minimum and maximum temperature range (gray shading) at the South and (d) North mooring sites, respectively. Individual thermistors have similar temperature patterns at the various heights (i.e., minimal vertical stratification, see Fig. 3). The solid black line in (c) and (d) denotes the depth-averaged, subtidal (33-h low-pass filtered) temperature. (e) North/south (positive, northward) and (f) east/west (positive, eastward) velocity contour maps for the North mooring site. The solid blue line in plots (e) and (f) denotes the location of the sea surface. (For interpretation of the references to color in this figure legend, the reader is referred to the web version of this article.)

The low-frequency (seasonal) nearshore temperature signal at each mooring site is positively correlated with the offshore seasonal temperature signal (Fig. 2c and d). During strong regional upwelling when the offshore thermocline shoals towards the surface, the nearshore temperature decreases. As the upwelling winds subside and the offshore thermocline deepens, the nearshore temperature increases and reaches its maximum around December. The vertical location of the nearshore temperature signal at the offshore mooring was calculated (i.e., vertical location in the offshore where the offshore temperature matched the nearshore temperature at each particular time) (Fig. 2b). The nearshore temperature signal typically matched the temperature signal seen in the top ~25 to 50 m of the offshore water column with the deepest depths seen during the winter months.

The nearshore temperature signal is also characterized by higher-frequency fluctuations, with daily temperature ranges across all depths often exceeding 6 °C (Fig. 2c and d). The high-frequency variability shows a distinct seasonal structure, with the largest fluctuations (i.e., range) seen during the summer months, gradually declining through the fall until reaching the smallest temperature range in the winter months. The high-frequency fluctuations start to increase again in the spring before reaching their summer maximum. We note that the change in the high-frequency variability appears to be controlled by the offshore vertical structure and thermocline location, as the water column stratification provides a wave guide for the internal waves, and the internal tide, onto the shelf. A comparison between the North and South mooring temperature suggests a similar seasonal signal and similar seasonal variations in the temperature range. The nearshore velocity signal at the North mooring also shows higher-frequency variability with a northwestward time-averaged velocity throughout the water column (Fig. 2e and f).

3.2. Tidal pumping and nearshore internal bores

Closer analysis of the nearshore temperature record reveals large-amplitude, semidiurnal temperature oscillations that appear to be coherent with the local sea surface height (Fig. 3). This coherence, as well as the structure of the features (described in detail below), suggests that they are the manifestation of the internal tide interacting with the canyon edge via tidal pumping (Shea and Broenkow, 1982; Petruncio et al., 1998, 2002). Spectral analysis of the surface tidal height shows a dominant peak at the semidiurnal frequency (M_2 tidal constituent), with a much smaller contribution to the total variance from the diurnal frequency component (Fig. 4a). The depth-averaged nearshore temperature signal at both moorings also reveals a dominant peak at the semidiurnal frequency (M_2 tidal constituent), with negligible contribution from the diurnal component (Fig. 4b).

Both temperature moorings show similar temperature patterns at the various heights throughout the bottom ~13 to 14 m of the water column, which is the extent of the vertical temperature measurements (Fig. 3b and c). The depth-averaged temperature will be used in subsequent analysis to describe the internal temperature dynamics since we are interested in describing the general characteristics of the temperature signal. The depth-averaged temperature ($<T>$, where $<>$ denotes a depth-averaged quantity over the vertical extent of the measurements) accurately depicts the dominant temporal variability of the temperature signals (Fig. 3b and c). In order to assess the spatial variability of the temperature signal across the canyon rim (i.e., different geographic locations near the canyon head), a coherence analysis was performed between the depth-averaged temperature at the North and South mooring sites. The two signals are significantly coherent across most of the frequency space with nearly no phase lag between the two signals (Fig. 5). The signals start to lose coherence at higher frequencies (periods of ~3 h), but the dominant temperature variability (e.g., lower frequencies such as the semidiurnal frequency) is comparable between the two sites. Similar results were obtained when assessing the coherence between the near-bottom temperature time series (0.9 and 1.5 mab at the South and North sites, respectively) and the shallowest temperature time series (13.1 and 13.7 mab at the South and North sites, respectively).

We test the hypothesis originally proposed by Shea and Broenkow (1982) that the nearshore temperature dynamics are controlled by a process termed tidal pumping (Petruncio et al., 1998, 2002). Fig. 3 illustrates that the tidal period pumping of the internal tide, which results in the nearshore temperature signal, is seemingly linked to the local sea surface height. During periods of rising surface tide (i.e., several hours before the high tide), cold–water surges are seen in the canyon rim temperature signal. These features deliver subthermocline water to the adjacent shelf, and will hereafter be referred to as internal bores (Walter et al. (2012) and the references therein). On the other hand, during the falling tide (i.e., several hours before the low tide) warm water reappears at the mooring sites.

A coherence analysis over the entire study period between the local sea surface height and the nearshore temperature signal reveals a statistically significant coherence at the semidiurnal

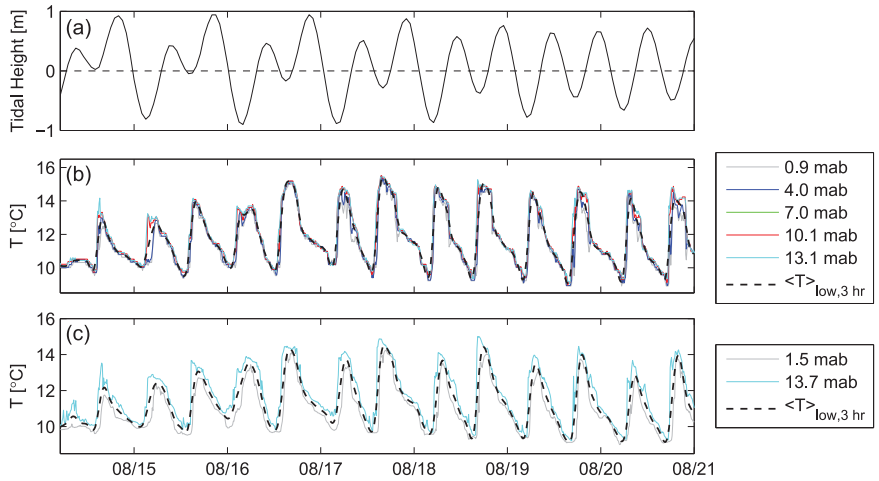

Fig. 3. Time series example from August 2012. (a) Sea surface tidal height where the time-mean has been removed. (b) Time series of temperature at various heights throughout the water column at the South and (c) North mooring sites, respectively. The dashed black line in (b) and (c) denotes the depth-averaged, 3-h low-pass filtered temperature used to identify the internal tide/bore phase in subsequent analysis.

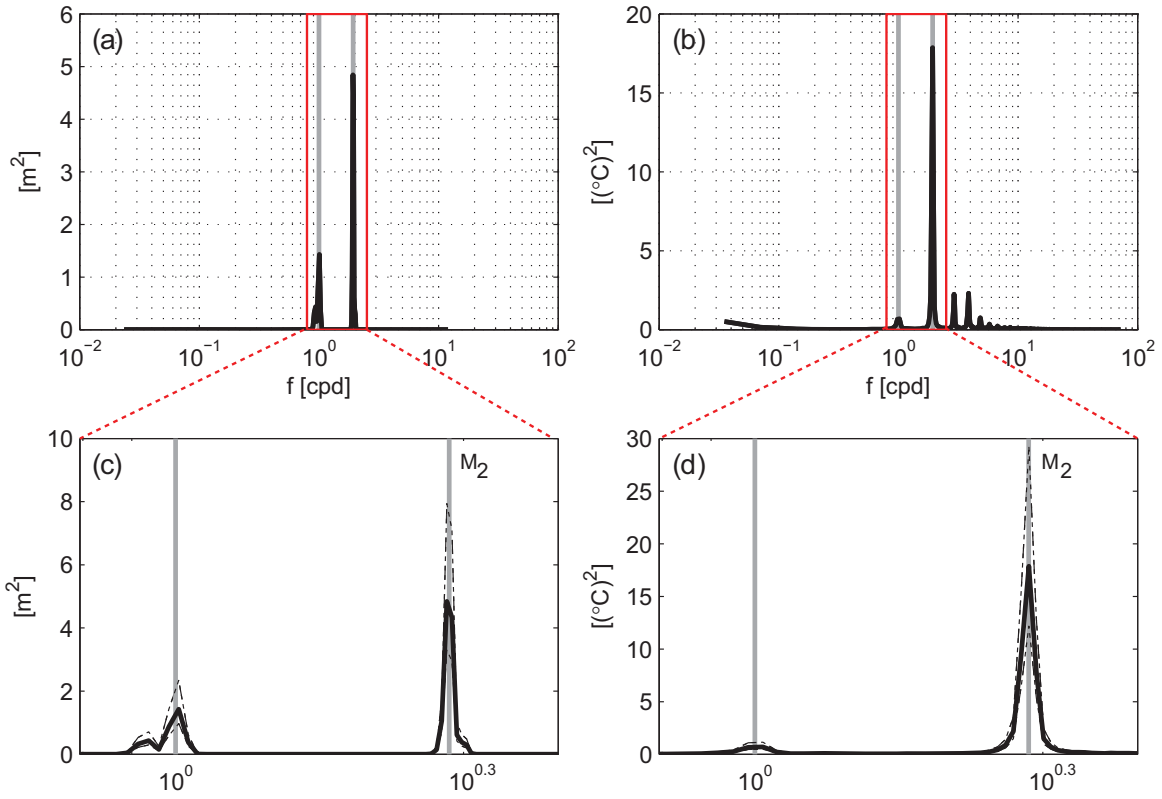

Fig. 4. Variance-preserving power spectra over the entire study period of the (a) sea surface tidal height and the (b) depth-averaged temperature from the South mooring. The red box in panels (a) and (b) denotes the zoomed in region shown in panels (c) and (d), respectively. The diurnal (24 h period) and semidiurnal (12.42 h period, M_2 tidal constituent) frequencies are shown as a dark gray line in each panel. The black dashed lines in panels (c) and (d) represent the upper and lower 90% confidence intervals. Similar temperature spectra were obtained from the North mooring. (For interpretation of the references to color in this figure legend, the reader is referred to the web version of this article.)

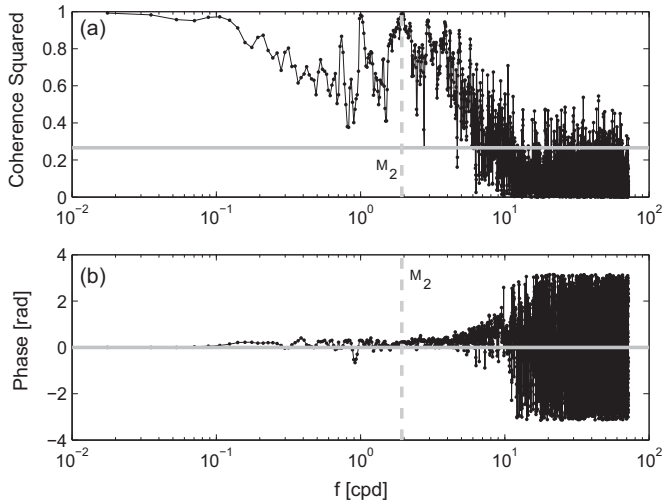

Fig. 5. (a) Coherence squared and (b) phase lag between the depth-averaged temperature at the North and South mooring sites. The 95% confidence level is shown as a gray line in (a). The location of the M_2 tidal component (~12.42 h period) is denoted by a dashed gray line. A positive phase lag at a given frequency indicates that the North mooring temperature lags the South mooring temperature.

frequency (M_2 tidal constituent) (Fig. 6). Analysis of the phase lag reveals that the temperature leads the tidal height by about 2.4 h, which is consistent with the cold (warm) water transitions appearing during the rising (falling) tide. This highlights that the nearshore temperature dynamics at the canyon edge and delivery of subthermocline waters to the adjacent shelf by internal bores may be locally predictable near the canyon rim. This is in contrast with previous observations tens of kilometers away from the canyon rim on the adjacent shelf in southern Monterey Bay, where the internal bores are typically not correlated with surface tides (Booth et al., 2012; Walter et al., 2012). This is likely attributable to background environmental conditions on the shelf (e.g., background currents and velocity shear, stratification, etc.) that have the ability to modulate the internal waves/bores as they propagate from the canyon rim to the adjacent shelf (Nash et al., 2012; Stastna and Walter, 2014; Walter et al., 2014b).

The observed internal bores (i.e., cold–water masses) at the canyon rim show a distinct asymmetry between the leading and trailing edges of individual bores (Fig. 3b and c). The leading edge of the bore is accompanied by a gradual cooling throughout the water column, as the cold subthermocline waters below the thermocline crest the canyon rim. This gradual cooling takes place over several hours and is followed by an extremely sharp warm front, as the displaced shelf waters return ("relax") to their original state (Pineda, 1994; Walter et al., 2012). In order to quantify the asymmetry and delineate the various phases of the bore, the time-derivative of temperature was calculated. The time-derivative was also low-pass filtered (3 h half-amplitude period) to reduce some of the higher-frequency variability and better delineate the bore phases. The derivative accurately captures the slow (fast) temperature changes [i.e., small negative (large positive) derivatives] associated with the leading (trailing) edge of the internal bores at the canyon rim and will be used in subsequent analysis to define the bore phase (Fig. 7).

The observed internal bores at the canyon rim follow the non-canonical structure observed by Walter et al. (2012) in southern Monterey Bay. Walter et al. (2012) investigated the non-canonical nature of internal bores using a numerical model and found that

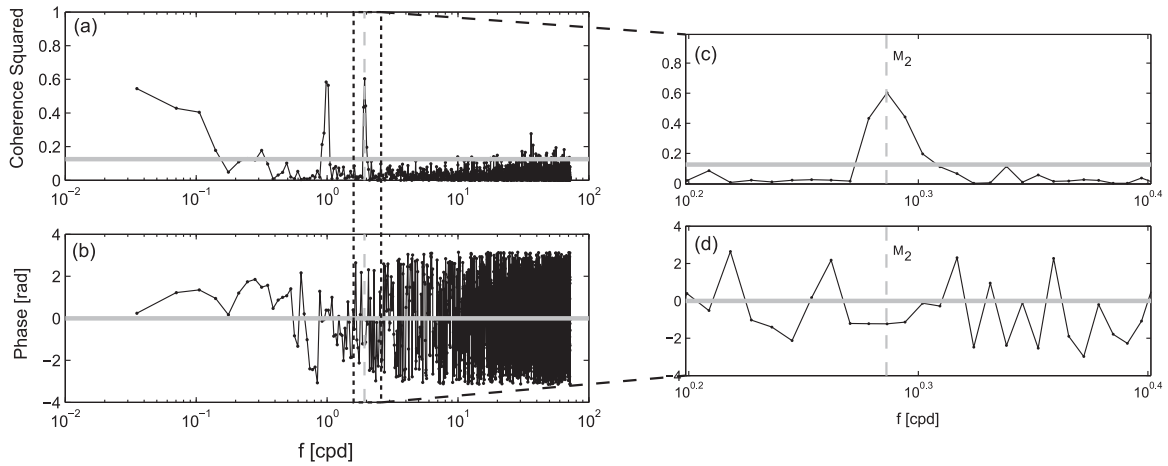

Fig. 6. (a) Coherence squared and (b) phase lag between the depth-averaged temperature at the South mooring and the sea surface height (i.e., tidal height). The 95% confidence level is shown as a gray line in (a). The location of the M_2 tidal component (~12.42 h period) is denoted by a dashed gray line. A positive phase lag at a given frequency indicates that the temperature lags sea surface height. Panels (c) and (d) denote the zoomed in region indicated by the dashed black box on panels in (a) and (b).

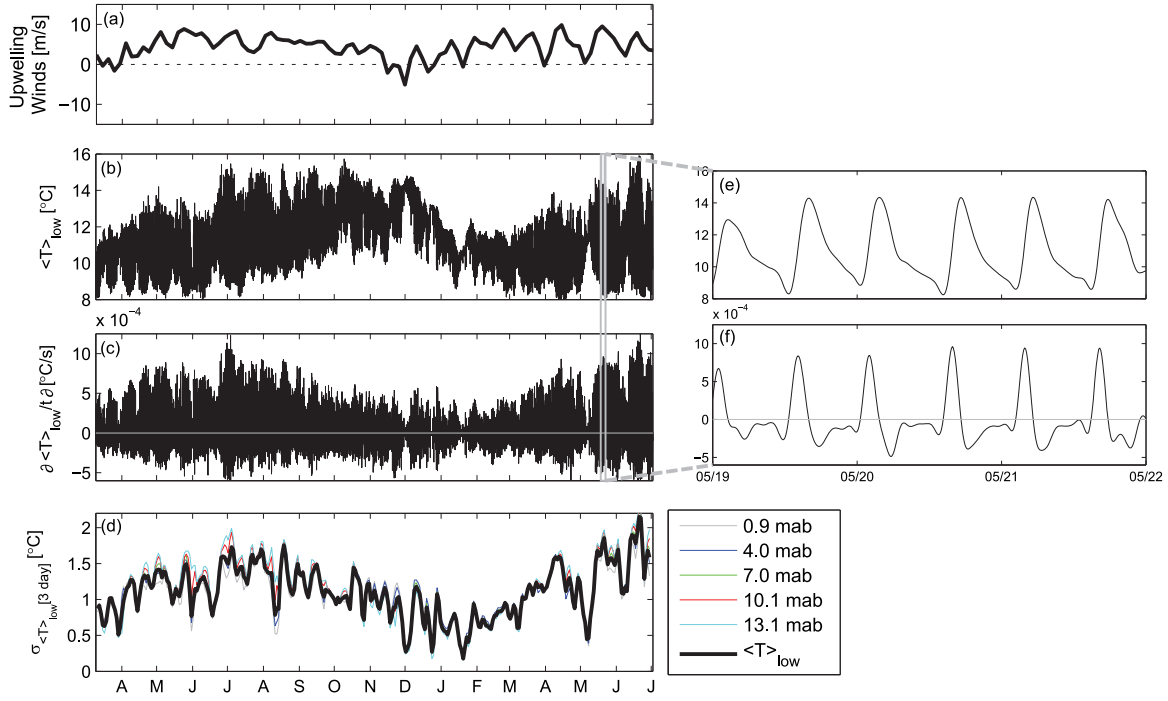

Fig. 7. Time series data over the entire 2012 to 2013 study period. (a) Regional upwelling favorable winds (positive) from NDBC buoy 46042 (10 day windowed-mean, as in Fig. 2a). (b) Depth-averaged, 3-h low-pass filtered temperature and the (c) time-derivative of the depth-averaged, 3-h low-pass filtered temperature used to identify the internal tide/bore phase at the South mooring. (d) Windowed-standard deviation of the depth-averaged temperature (black) and the temperature at various heights above the bed (colored lines) from the South mooring used to identify the bore strength. Windowed values were calculated using 3 day windows with 50% overlap. Panels (e) and (f) highlight the zoomed in region of the gray box in panels (b) and (c). (For interpretation of the references to color in this figure legend, the reader is referred to the web version of this article.)

the structure was explained by the steep bathymetric slope in the southern Monterey Bay region and dependence on the internal Iribarren number,

$$\xi = \frac{s}{\left(\frac{a}{\lambda}\right)^{\frac{1}{2}}}, \tag{2}$$

where s is the bathymetric slope, and a and λ are the offshore amplitude and wavelength of the incoming internal wave, respectively (Boegman et al., 2005). For a gentle bathymetric slope, the model produced a nearshore temperature signal with a more abrupt cooling period followed by a gradual warming (canonical bore, see Leichter et al. (1996), Martini et al. (2013), Washburn and McPhee-Shaw (2013), etc.). For a steep bathymetric slope, the model generated a nearshore temperature signal with a more gradual cooling and sharp warming like the features in this study (non-canonical bore, see Pineda (1994), Walter et al. (2012, 2014a, 2014b), etc.). The steep bathymetric slope at the head of the canyon rim likely controls the structure of the internal bores. Note that while the bore structure is influenced by the local bathymetry, the offshore vertical temperature structure and stratification determine the resultant nearshore internal bore patterns and high-frequency variability. It is also this stratification and resulting internal wave guide that allows for the pulsed delivery of sub-thermocline waters to the nearshore by internal bores.

3.3. Seasonality of internal bores

The aforementioned seasonality in the wind-driven upwelling and offshore stratification/thermocline depth is linked to the strength of the internal bores and semidiurnal temperature variability in the nearshore. Fig. 7c highlights the windowed-standard deviation of the nearshore depth-averaged temperature (3 day windows with 50% overlap; results were not sensitive to the choice of window used). The windowed-standard deviation captures the variation in the semidiurnal temperature fluctuations driven by the internal tide. Temperature variability peaks during the summer months when the offshore thermocline shoals towards the surface due to increased regional upwelling. As the upwelling winds weaken and the offshore thermocline deepens throughout the fall months, the windowed-standard deviation gradually declines until reaching a minimum in the winter months.

Wavelet analysis was utilized to investigate the frequency–time variability of the canyon rim temperature signal. Fig. 8 shows that the variance in the temperature signal is dominated by the semidiurnal frequency component over time, with a much smaller contribution from lower frequencies (including the diurnal band). Scale-averaged wavelet power in the semidiurnal band (11–14 h periods), which effectively isolates the contribution from the semidiurnal internal tide to the total variance, reveals a similar seasonal trend as the windowed-standard deviation. During the summer (winter) months, the semidiurnal temperature variability is at its maximum (minimum). Ramifications of the seasonality and the resulting delivery of subthermocline waters to the nearshore are discussed below.

3.4. Velocity dynamics and delivery of subthermocline waters

In addition to driving transient temperature fluctuations at the nearshore canyon rim, the internal bores force ephemeral onshelf (offshelf) flows during the leading (trailing) edge of the features. Fig. 9 shows example bore events from October 2012 and highlights that during periods of nearshore cooling (slow declines in the nearshore temperature; leading edge) the velocities at the North site are directed northwestward, or onto the adjacent shelf, over the bottom portion of the water column (i.e., vertical extent of the temperature measurements). This is contrasted with periods of nearshore warming (fast increases in the nearshore temperature; trailing edge) where the velocities are directed southeastward or southwestward, or back into the canyon. The internal bores also drive substantial vertical velocity shear, especially during the trailing edge of the bores, which may lead to enhanced turbulent mixing in the stratified interior (cf. Walter et al. (2012, 2014b)).

In order to generalize the aforementioned velocity field observations over the entire velocity record, the time-derivative of the depth-averaged temperature was used to identify the leading and trailing edges (phases) of the bore (see previous section). Fig. 10 displays a scatterplot of the bottom-averaged (i.e., vertical extent of the temperature measurements) north and east velocity fields from the North mooring. The velocity scatterplot is colored according to the bore phase at the North mooring site at the time of the respective velocity measurement. It is clear that the leading (cooling period) edge of the bore at the North mooring typically drives northward velocities over the bottom portion of the water column, and provides a mechanism for the delivery of subthermocline waters to the adjacent shelf. The trailing (warming period) edge of the bore drives flow back into the canyon (i.e., southward) at this location.

Fig. 11 shows the windowed-mean (3 day windows, 50% overlap) bottom-averaged horizontal velocity magnitude as a function of the windowed-standard deviation (3 day windows, 50% overlap) of the depth-averaged temperature (i.e., bore strength proxy). Increases (decreases) in bore strength are linked to increases (decreases) in the horizontal velocity magnitude at the canyon rim. Note that Fig. 11 uses the North mooring velocity measurements in conjunction with the South mooring temperature measurements because of the increased time of overlap between the respective measurements (Fig. 2). This is justified given the significant coherence between the North and South temperature

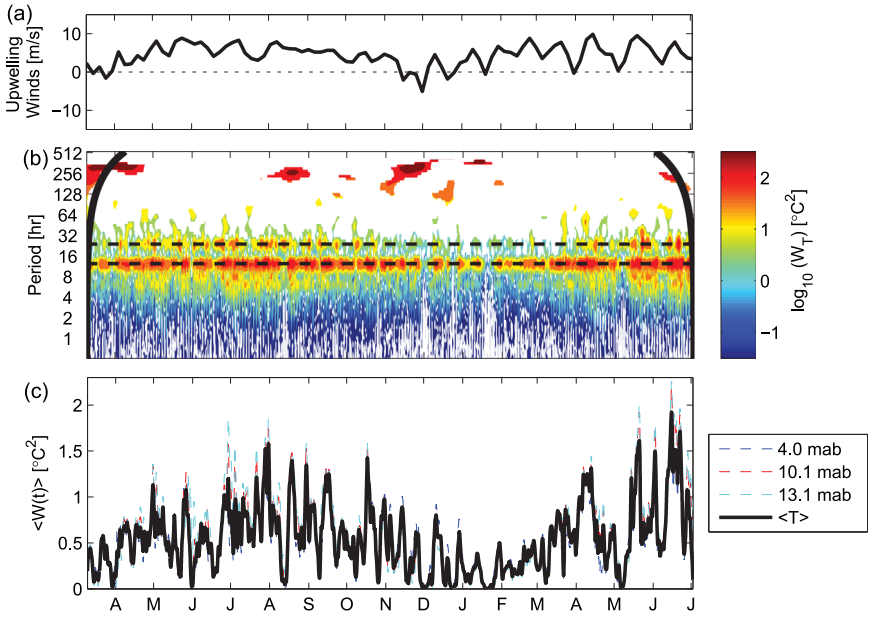

Fig. 8. (a) Regional upwelling favorable winds (positive) from NDBC buoy 46042 (10 day windowed-mean, as in Fig. 2a) from 2012 to 2013. (b) Wavelet power spectrum of the depth-averaged temperature at the South mooring site. Thick black lines on both ends of the spectrum indicate the "cone of influence" where edge effects become important. Only the wavelet power that is significant at the 90% confidence level is shown. The dashed black lines denote the diurnal (24 h) and semidiurnal (M_2 tidal component, ~12.42 h) periods. (c) Scale-averaged wavelet power between 11 and 14 h isolating the semidiurnal internal tide band for the depth-averaged temperature at the South mooring (black line). The scale-averaged power for other temperature heights above the bed (those with continuous data over the entire study period) are also shown (dashed colored lines). (For interpretation of the references to color in this figure legend, the reader is referred to the web version of this article.)

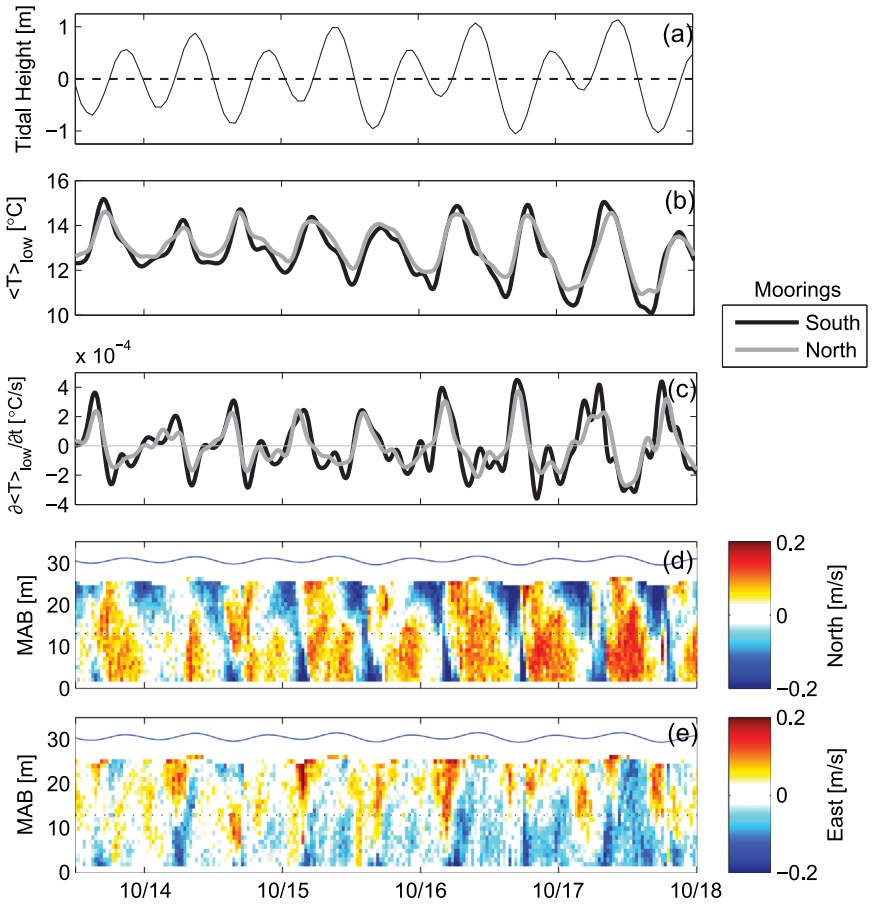

Fig. 9. Time series example from October 2012. (a) Sea surface tidal height where the time-mean has been removed. (b) Depth-averaged, 3-h low-pass filtered temperature and the (c) time-derivative of the depth-averaged, 3-h low-pass filtered temperature used to identify the internal tide/bore phase at the South (black) and North (gray) mooring locations. (d) North/south (positive, northward) and (e) east/west (positive, eastward) velocity contour maps for the North mooring site. The solid blue line in plots (d) and (e) denotes the location of the sea surface. (For interpretation of the references to color in this figure legend, the reader is referred to the web version of this article.)

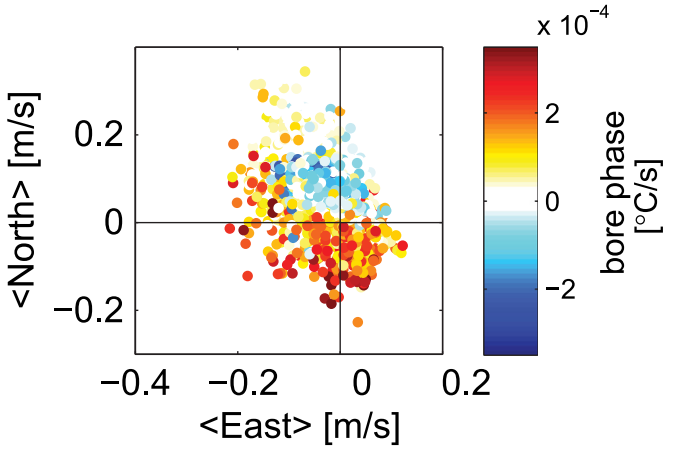

Fig. 10. Scatterplot of the bottom-averaged north and east velocities from the North mooring ADP. The vertical averaging was done over the bottom 14.1 m of the water column, where 14.1 m corresponds to the ADP bin that was closest to the vertical extent of the temperature measurements. The velocity scatterplot is colored according to the internal tide/bore phase at the North mooring site at the time of the respective velocity measurement. The internal tide/bore phase was calculated using the time-derivative of the depth-averaged, 3-h low-pass filtered temperature from the North site (bore phase $= \partial\langle T\rangle_{low}/\partial t$). Overlapping between colored circles is minimal and does not affect any of the conclusions. (For interpretation of the references to color in this figure legend, the reader is referred to the web version of this article.)

measurements (Fig. 5). Analysis of the windowed-mean, bottom-averaged north and east velocity components at the North mooring site, respectively, as a function of time (not shown) show that the north (east) component of velocity is always positive (negative). This indicates that on average the flow is directed northwestward over the bottom portion of the water column and onto the adjacent shelf at this location. We surmise that the asymmetry in the internal bore structure, and in particular the long cooling period (leading edge) relative to the fast warming period (trailing edge), results in this net flow onto the shelf.

3.5. Ecological implications

The observed velocity dynamics and seasonality of the internal bores at the canyon head have tremendous implications for the nearshore coastal environment. The internal tide interacting with the canyon head results in a pulsed delivery of subthermocline waters onto the adjacent shelf and provides a means for the cross-shelf exchange of these waters. The subthermocline waters are rich in nutrients and contribute to the flux of nutrients to the nearshore, thereby helping to fuel nearshore kelp forest ecosystems and communities; however, the subthermocline waters are also low in DO and pH (Leichter et al., 1996; Booth et al., 2012; Washburn and McPhee-Shaw, 2013). While it is well-documented that seasonal upwelling contributes to nearshore DO variability and the potential development of coastal hypoxia, as well as pH variability and ocean acidification processes, this research suggests that the internal tide interacting with the canyon rim may contribute to rapid fluctuations in DO/pH in the nearshore with extremely fast onset times of these low DO/pH waters relative to those expected under upwelling alone (Chan et al., 2008; Booth et al., 2012; Walter et al., 2014b). The internal boluses also may

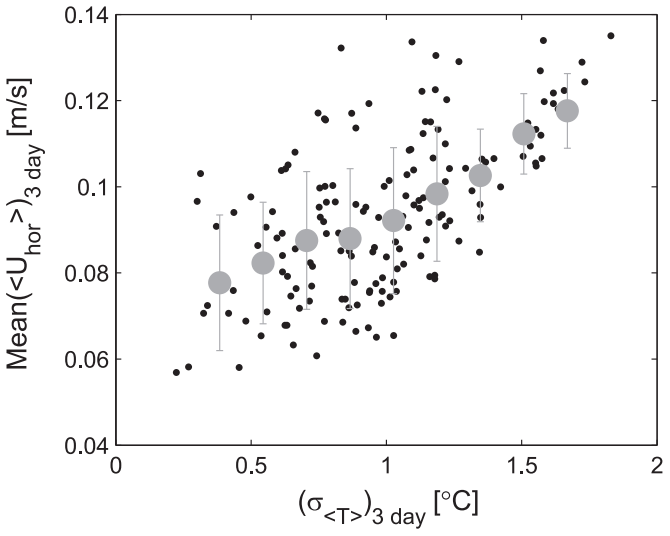

Fig. 11. Scatterplot of the windowed-mean, bottom-averaged horizontal velocity magnitude from the North mooring ADP as a function of the window-standard deviation of the depth-averaged temperature from the South mooring. Windowed values were calculated using 3 day windows with 50% overlap. The vertical averaging of the ADP was done over the bottom 14.1 m of the water column, where 14.1 m corresponds to the ADP bin that was closest to the vertical extent of the temperature measurements. The small black dots denote the windowed/vertically-averaged values, while the larger gray dots signify the bin-average of the windowed/vertically-averaged values (i.e., small black dots that represent windowed/vertically-averaged values were grouped into equally spaced bins across the horizontal axis and averaged to produce the large gray bin-averaged dots). The error bars on the larger gray dots represent the standard deviation of the binned results (i.e., standard deviation of all the windowed/vertically averaged values within that particular bin). The North mooring velocity measurements were used in conjunction with the South mooring temperature measurements because of the increased time of overlap between the respective measurements (Fig. 2). This is justified given the significant coherence between the North and South temperature measurements (Fig. 5).

contribute to the cross-shelf transport (Walter et al., 2014b) of larvae by delivering these organisms from the ambient coastal shelf waters adjacent to the canyon region to their natal nearshore habitats located in shallower subtidal and intertidal environments (Pineda, 1994), a process that may be important for connectivity and recruitment.

Moreover, the seasonality of the internal bores must be taken into account when assessing the supply of deep waters to the nearshore. During the summer months, not only are the bores stronger (i.e., larger temperature swings), but the average nearshore temperatures are also at their lowest levels due to the shoaling of the offshore thermocline. The effect of annual extreme low DO/pH levels due to the seasonally shallow offshore thermocline during the summer months, combined with increased bore strength that results in large swings in these parameters, may prove particularly stressful to organisms sensitive to these water column parameters. This contribution extends the results of previous studies (Cheriton et al., 2014b; Walter et al., 2014b) that highlight how upwelling, and the subsequent modulation of stratification, sets the ability of internal waves to propagate onto the shelf and deliver cold–water masses to the coastal environment. Consideration of upwelling seasonality is thus not only important for assessing low-frequency changes to background environmental conditions and water-column properties, as has been previously demonstrated in the literature (Pennington and Chavez, 2000), but it is also significant for higher-frequency changes and the onset time of these deep water masses (Walter et al., 2014b). This upwelling seasonality and the modulation of internal waves may prove significant in assessing larval transport, coastal hypoxia, and ocean acidification processes.

4. Conclusion

This study took advantage of long-term moored measurements made in shallow waters (~30 m) at the head of the MSC in order to characterize the oceanographic environment and internal tide at this location. We show that the interaction of the internal tide with the canyon rim results in a semidiurnal tidal period pumping of cold–water masses onto the adjacent shelf (internal bores). These internal bores are significantly coherent with the surface tide and result in the regular delivery of subthermocline waters onto the adjacent shelf. The spatial variability of these features is minimal across two sites on opposite sides of the canyon head, as evidenced by the significant coherence across most of the frequency space. The temporal variability and seasonality of these features was assessed, and results illustrate elevated semidiurnal temperature variance during the summer months when strong wind-driven upwelling causes the offshore thermocline to shoal towards the surface. Temperature variability was weakest during the winter months when the offshore thermocline deepened due to weakening upwelling favorable winds.

The observed internal bores are characterized by a distinct asymmetry between their leading and trailing edges. The arrival of the bores and subthermocline waters are typified by a gradual cooling period, which is followed by the relaxation of the bore and a sharp warming period. Analysis of the velocity data illustrated bottom-averaged flows onto the shelf (back into the canyon) during the leading (trailing) edges of the bores, as well as enhanced velocities during periods of strong internal bore activity. This implies that the semidiurnal internal bores are the dominant mode of physical variability at the canyon head and a first-order control on the delivery of subthermocline waters to the adjacent shelf. Moreover, the temperature variability in the nearshore appears to be at least partially controlled by the offshore response (i.e., stratification strength and thermocline location) to seasonality in wind-driven upwelling. It is clear that the seasonality of the internal bores at the canyon rim needs to be considered when assessing the delivery of subthermocline waters to the adjacent shelf, a process that has implications for coastal hypoxia, ocean acidification, and the design of future desalination plants that seek to access these deep waters.

Internal bores are common along continental margins around the world (Shea and Broenkow, 1982; Pineda, 1994; Leichter et al., 1996; Colosi et al., 2001; Klymak and Moum, 2003; Hosegood and Van Haren, 2004; Nam and Send, 2011; Cheriton et al., 2014a, 2014b; Walter et al., 2012, 2014a, 2014b; Suanda et al., 2014; etc.). While there have been several observations of elevated semidiurnal internal tide energy at other canyon head locations (Petruncio et al., 1998 and the references therein; Hall et al. (2014) and the references therein), further observations are required to extend the results presented here to other nearshore canyon head regions. This is particularly true with respect to the conclusions drawn on the predictability of the features (i.e., coherence of the temperature signal with the surface tide), as well as factors influencing the delivery of subthermocline water to the continental shelf (i.e., wind-driven upwelling, offshore stratification, bathymetric slope and bore structure, etc.). The MSC is likely a key contributor to the delivery of subthermocline waters to the nearshore regions around the canyon head, given its close proximity to the shore. In addition to providing a mechanism for the cross-shelf transport of various scalars, these shoaling internal waves (bores) also likely contribute to the dissipation of turbulent kinetic energy and vertical mixing of scalars at various shelf locations (Arthur and Fringer, 2014; Walter et al., 2014a, 2014b). Future work should focus on the fate and evolution of the cold–water masses, as well as the resulting effect on various physical and biological processes (e.g., DO/pH variability, larval transport, vertical mixing, cross-shelf exchange, etc.).

Acknowledgments

The authors acknowledge the Monterey Bay Aquarium Research Institute (MBARI) for providing the M1 mooring data and Jason Adelaars for downloading this data. The authors also acknowledge helpful discussions with Robert Arthur and John Steinbeck. Early discussions with Erika McPhee-Shaw and Leslie Rosenfeld also contributed to the development of the work. Special thanks to John Hedgepeth, Gery Cox, and the scientists at Tenera Environmental for their efforts in field work and data collection. This work was supported by DeepWater Desal, LLC; Monterey Peninsula Water Management District; and the Moss Landing Power Plant (Dynergy Moss Landing, LLC). Bathymetry data used in this study were acquired, processed, archived, and distributed by the Seafloor Mapping Lab of California State University Monterey Bay.

References

Arthur, R.S., Fringer, O.B., 2014. The dynamics of breaking internal solitary waves on slopes. J. Fluid Mech., 360–398. http://dx.doi.org/10.1017/jfm.2014.641.

Boegman, L., Ivey, G.N., Imberger, J., 2005. The degeneration of internal waves in lakes with sloping topography. Limnol. Oceanogr. 50, 1620–1637. http://dx.doi.org/10.4319/lo.2005.50.5.1620.

Boehm, A.B., Sanders, B.F., Winant, C.D., 2002. Cross-shelf transport at Huntington Beach. Implications for the fate of sewage discharged through an offshore ocean outfall. Environ. Sci. Technol. 36, 1899–1906. http://dx.doi.org/10.1021/es0111986.

Booth, J.A.T., McPhee-Shaw, E.E., Chua, P., Kingsley, E., Denny, M., Phillips, R., Bograd, S.J., Zeidberg, L.D., Gilly, W.F., 2012. Natural intrusions of hypoxic, low pH water into nearshore marine environments on the California coast. Cont. Shelf Res. 45, 108–115. http://dx.doi.org/10.1016/j.csr.2012.06.009.

Breaker, L.C., Broenkow, W.W., 1994. The circulation of Monterey Bay and related processes. Oceanogr. Mar. Biol. an Annu. Rev 32, 1–64.

Carter, G.S., 2010. Barotropic and baroclinic M_2 tides in the Monterey Bay Region. J. Phys. Oceanogr. 40, 1766–1783. http://dx.doi.org/10.1175/2010JPO4274.1.

Carter, G.S., Gregg, M.C., 2002. Intense, variable mixing near the head of Monterey Submarine Canyon. J. Phys. Oceanogr. 32, 3145–3165. http://dx.doi.org/10.1175/1520-0485(2002)032 < 3145:IVMNTH > 2.0.CO;2.

Carter, G.S., Gregg, M.C., Lien, R.C., 2005. Internal waves, solitary-like waves, and mixing on the Monterey Bay shelf. Cont. Shelf Res. 25, 1499–1520. http://dx.doi.org/10.1016/j.csr.2005.04.011.

Chan, F., Barth, J. a, Lubchenco, J., Kirincich, a, Weeks, H., Peterson, W.T., Menge, B. a, 2008. Emergence of anoxia in the California current large marine ecosystem. Science 319, 920. http://dx.doi.org/10.1126/science.1149016.

Cheriton, O.M., McPhee-Shaw, E.E., Shaw, W.J., Stanton, T.P., Bellingham, J.G., Storlazzi, C.D., 2014a. Suspended particulate layers and internal waves over the southern Monterey Bay continental shelf: An important control on shelf mud belts? J. Geophys. Res. Oceans 119, 428–444. http://dx.doi.org/10.1002/2013JC009360.

Cheriton, O.M., McPhee-Shaw, E.E., Storlazzi, C.D., Rosenberger, K.J., Shaw, W.J., Raanan, B.Y., 2014b. Upwelling rebound, ephemeral secondary pycnoclines, and the creation of a near-bottom wave guide over the Monterey Bay continental shelf. Geophys. Res. Lett. 41, 8503–8511. http://dx.doi.org/10.1002/2014GL061897.

Colosi, J. a, Beardsley, R.C., Lynch, J.F., Gawarkiewicz, G., Chiu, C.-S., Scotti, A., 2001. Observations of nonlinear internal waves on the outer New England continental shelf during the summer Shelfbreak Primer study. J. Geophys. Res. 106, 9587. http://dx.doi.org/10.1029/2000JC900124.

Davis, K.A., Leichter, J.J., Hench, J.L., Monismith, S.G., 2008. Effects of western boundary current dynamics on the internal wave field of the Southeast Florida shelf. J. Geophys. Res. Ocean 113, C09010. http://dx.doi.org/10.1029/2007JC004699.

Emery, W.J., Thomson, R.E., 2001. Data Analysis Methods in Physical Oceanography. second and revised edition, Marine Ecology Progress Series. Elsevier, Amsterdam, 638 pp.

Farge, M., 1992. Wavelet transforms and their applications to turbulence. Annu. Rev. Fluid Mech. 24, 395–457. http://dx.doi.org/10.1146/annurev.fluid.24.1.395.

García-Reyes, M., Largier, J.L., 2012. Seasonality of coastal upwelling off central and northern California: New insights, including temporal and spatial variability. J. Geophys. Res. . http://dx.doi.org/10.1029/2011JC007629

Garrett, C., Kunze, E., 2007. Internal tide generation in the deep ocean. Annu. Rev. Fluid Mech. 39, 57–87. http://dx.doi.org/10.1146/annurev.fluid.39.050905.110227.

Hall, R.A., Alford, M.H., Carter, G.S., Gregg, M.C., Lien, R.C., Wain, D.J., Zhao, Z., 2014. Transition from partly standing to progressive internal tides in Monterey Submarine Canyon. Deep. Res. Part II Top. Stud. Oceanogr 104, 164–173. http://dx.doi.org/10.1016/j.dsr2.2013.05.039.

Hall, R. a, Carter, G.S., 2011. Internal Tides in Monterey Submarine Canyon. J. Phys. Oceanogr. 41, 186–204. http://dx.doi.org/10.1175/2010JPO4471.1.

Hosegood, P., Van Haren, H., 2004. Near-bed solibores over the continental slope in the Faeroe-Shetland Channel in:. Deep-Sea Res. Part II: Top. Stud. Oceanogr., 2943–2971. http://dx.doi.org/10.1016/j.dsr2.2004.09.016.

Jachec, S.M., Fringer, O.B., Gerritsen, M.G., Street, R.L., 2006. Numerical simulation of internal tides and the resulting energetics within Monterey Bay and the surrounding area. Geophys. Res. Lett. 33, 2–5. http://dx.doi.org/10.1029/2006GL026314.

Kang, D., Fringer, O., 2012. Energetics of barotropic and baroclinic tides in the Monterey Bay Area. J. Phys. Oceanogr. 42, 272–290. http://dx.doi.org/10.1175/JPO-d-11-039.1.

Kelly, S.M., Nash, J.D., 2010. Internal-tide generation and destruction by shoaling internal tides. Geophys. Res. Lett. 37, 1–5. http://dx.doi.org/10.1029/2010GL045598.

Klymak, J.M., Moum, J.N., 2003. Internal solitary waves of elevation advancing on a shoaling shelf. Geophys. Res. Lett. . http://dx.doi.org/10.1029/2003GL017706

Kunze, E., Rosenfeld, L.K., Carter, G.S., Gregg, M.C., 2002. Internal waves in Monterey Submarine Canyon. J. Phys. Oceanogr. 32, 1890–1913. http://dx.doi.org/10.1175/1520-0485(2002)032 < 1890:IWIMSC > 2.0.CO;2.

Leichter, J.J., Wing, S.R., Miller, S.L., Denny, M.W., 1996. Pulsed delivery of subthermocline water to Conch Reef (Florida Keys) by internal tidal bores. Limnol. Oceanogr. 41, 1440–1501. http://dx.doi.org/10.4319/lo.1996.41.7.1490.

Martini, K.I., Alford, M.H., Kunze, E., Kelly, S.M., Nash, J.D., 2013. Internal bores and breaking internal tides on the Oregon continental slope. J. Phys. Oceanogr. 43, 120–139. http://dx.doi.org/10.1175/JPO-d-12-030.1.

Nam, S., Send, U., 2011. Direct evidence of deep water intrusions onto the continental shelf via surging internal tides. J. Geophys. Res. 116, 1–15. http://dx.doi.org/10.1029/2010JC006692.

Nash, J., Shroyer, E., Kelly, S., Inall, M., 2012. Are any coastal internal tides predicatble? Oceanography 25, 80–95. http://dx.doi.org/10.5670/oceanog.2012.44.

Pennington, J.T., Chavez, F.P., 2000. Seasonal fluctuations of temperature, salinity, nitrate, chlorophyll and primary production at station H3/M1 over 1989–1996 in Monterey Bay, California. Deep. Res. Part II Top. Stud. Oceanogr. 47, 947–973. http://dx.doi.org/10.1016/S0967-0645(99)00132-0.

Petruncio, E., Paduan, J.D., Rosenfeld, L.K., 2002. Numerical simulations of the internal tide in a submarine canyon. Ocean Model. 4, 221–248. http://dx.doi.org/10.1016/S1463-5003(02)00002-1.

Petruncio, E.T., Rosenfeld, L.K., Paduan, J.D., 1998. Observations of the internal tide in Monterey Canyon. J. Phys. Oceanogr. 28, 1873–1903. http://dx.doi.org/10.1175/1520-0485(1998)028 < 1873:OOTITI > 2.0.CO;2.

Pineda, J., 1994. Internal tidal bores in the nearshore: warm–water fronts, seaward gravity currents and the onshore transport of neustonic larvae. J. Mar. Res. 52, 427–458. http://dx.doi.org/10.1357/0022240943077046.

Rosenfeld, L.K., Schwing, F.B., Garfield, N., Tracy, D.E., 1994. Bifurcated flow from an upwelling center: a cold water source for Monterey Bay. Cont. Shelf Res. 14, 931–964. http://dx.doi.org/10.1016/0278-4343(94)90058-2.

Send, U., Beardsley, R.C., Winant, C.D., 1987. Relaxation from upwelling in the Coastal Ocean Dynamics Experiment. J. Geophys. Res. Ocean 92 (C2), 1683–1698.

Shea, R.E., Broenkow, W.W., 1982. The role of internal tides in the nutrient enrichment of Monterey Bay, California. Estuar. Coast. Shelf Sci. 15, 57–66. http://dx.doi.org/10.1016/0272-7714(82)90036-1.

Smith, D.P., Ruiz, G., Kvitek, R., Iampietro, P.J., 2005. Semiannual patterns of erosion and deposition in upper Monterey Canyon from serial multibeam bathymetry. Bull. Geol. Soc. Am. 117, 1123–1133. http://dx.doi.org/10.1130/B25510.1.

Stastna, M., Walter, R., 2014. Transcritical generation of nonlinear internal waves in the presence of background shear flow. Phys. Fluids 26, 086601. http://dx.doi.org/10.1063/1.4891871.

Storlazzi, C.D., McManus, M. a, Figurski, J.D., 2003. Long-term, high-frequency current and temperature measurements along central California: insights into upwelling/relaxation and internal waves on the inner shelf. Cont. Shelf Res. 23, 901–918. http://dx.doi.org/10.1016/S0278-4343(03)00045-1.

Suanda, S.H., Barth, J.A., Holman, R.A., Stanley, J., 2014. Shore-based video observations of nonlinear internal waves across the inner shelf. J. Atmos. Ocean. Technol. 31, 714–728. http://dx.doi.org/10.1175/JTECH-d-13-00098.1.

Torrence, C., Compo, G.∼P., 1998. A practical guide to wavelet analysis. BAMS 79, 61. http://dx.doi.org/10.1175/1520-0477(1998)079 < 0061:APGTWA > 2.0.CO;2.

Venayagamoorthy, S.K., Fringer, O.B., 2007. On the formation and propagation of nonlinear internal boluses across a shelf break. J. Fluid Mech. 577, 137. http://dx.doi.org/10.1017/S0022112007004624.

Walter R.K., Woodson C.B., Arthur R.S., Fringer O.B. and Monismith S.G., Nearshore internal bores and turbulent mixing in southern Monterey Bay, J. Geophys. Res. Ocean. 117, C07017, 2012, http://dx.doi.org/10.1029/2012JC008115.

Walter, R.K., Nidzieko, N.J., Monismith, S.G., 2011. Similarity scaling of turbulence spectra and cospectra in a shallow tidal flow. J. Geophys. Res. Oceans 116, 1–14. http://dx.doi.org/10.1029/2011JC007144.

Walter, R.K., Squibb, M.E., Woodson, C.B., Koseff, J.R., Monismith, S.G., 2014a. Stratified turbulence in the nearshore coastal ocean: Dynamics and evolution in the presence of internal bores. J. Geophys. Res. Oceans 119, 8709–8730. http://dx.doi.org/10.1002/2014JC010396.

Walter, R.K., Woodson, C.B., Leary, P.R., Monismith, S.G., 2014b. Connecting wind-driven upwelling and offshore stratification to nearshore internal bores and oxygen variability. J. Geophys. Res. Oceans 119, 3517–3534. http://dx.doi.org/10.1002/2014JC009998.

Washburn, L., McPhee-Shaw, E.E., 2013. Coastal transport processes affecting inner-

shelf ecosystems in the California. Curr. Syst. Oceanogr. 26, 34–43. http://dx.doi.org/10.5670/oceanog.2013.43.
Wong, S.H.C., Santoro, A.E., Nidzieko, N.J., Hench, J.L., Boehm, A.B., 2012. Coupled physical, chemical, and microbiological measurements suggest a connection between internal waves and surf zone water quality in the Southern California Bight. Cont. Shelf Res. 34, 64–78. http://dx.doi.org/10.1016/j.csr.2011.12.005.
Woodson, C.B., Barth, J.A., Cheriton, O.M., McManus, M.A., Ryan, J.P., Washburn, L., Carden, K.N., Cheng, B.S., Fernandes, J., Garske, L.E., Gouhier, T.C., Haupt, A.J., Honey, K.T., Hubbard, M.F., Iles, A., Kara, L., Lynch, M.C., Mahoney, B., Pfaff, M., Pinsky, M.L., Robart, M.J., Stewart, J.S., Teck, S.J., True, A., 2011. Observations of internal wave packets propagating along-shelf in northern Monterey Bay. Geophys. Res. Lett. 38. http://dx.doi.org/10.1029/2010GL045453.
Zhao, Z., Alford, M.H., Lien, R.-C., Gregg, M.C., Carter, G.S., 2012. Internal tides and mixing in a submarine canyon with time-varying stratification. J. Phys. Oceanogr. 42, 2121–2142. http://dx.doi.org/10.1175/JPO-d-12-045.1.